Hybrid Crystalline sp^2-sp^3 Carbon as a High-Efficiency Solar Cell Absorber

Yue-Yu Zhang[1,2], Shiyou Chen[3], Hongjun Xiang[1,2], Xin-Gao Gong[1,2*]

[1]*Key Laboratory for Computational Physical Sciences (MOE), State Key Laboratory of Surface Physics, Department of Physics, Fudan University, Shanghai 200433, China*
[2]*Collaborative Innovation Center of Advanced Microstructures, Nanjing, 210093, China*
[3]*Key Laboratory of Polar Materials and Devices (MOE), East China Normal University, Shanghai 200241, China*

*E-mail: xggong@fudan.edu.cn

Abstract

Carbon is a versatile element that has allotropes with both sp^2 (graphene) and sp^3 (diamond) bonding. However, none of the allotropes can be used as light-absorber materials in solar cells due to either too large or too small band gap. Here, we propose a novel concept that enables a tunable band gap of carbon phases with sp^2 carbon atoms within a sp^3 carbon structure. The tunability is due to the quantum confinement effect. By embedding the sp^2 atoms within the sp^3 structure, we can design new carbon allotropes with ideal optical properties for optoelectronic applications. Five carbon allotropes incorporated this structural feature were identified by combining this new concept with our freshly developed multi-objective inverse band structure design approach. They all have proper band gaps for optical absorption, and the simulated photovoltaic efficiency of C_{10}-C is even higher than conventional absorber materials such as GaAs, which indicates that C_{10}-C with mixed sp^2-sp^3 hybridization may have potential application as light-absorber material in electronic and optoelectronic devices.

I. Introduction

Carbon is a versatile element, whose electronic states allow for sp^3, sp^2 and even *sp* hybridization. Hence, carbon can form many allotropes (graphite, diamond, fullerenes, nanotubes, etc.) with various micro-textures (more or less ordered), different dimensionalities (from 0 to 3D), and a rich variety of electronic structures (from metal to insulator)[1-4]. The exploration of new carbon allotropes has been the focus of numerous theoretical and experimental investigations because of their importance in both fundamental science and potential practical applications[5-11]. The two most stable phases of carbon, i.e., sp^3 hybridized diamond and sp^2 hybridized graphite (graphene), have a wide band gap (5.5 eV) and a zero gap, respectively. Moreover, all the recently predicted sp^3 hybridized carbon allotropes[9, 12-15] have large band gaps. Although carbon is abundant, cheap, nontoxic, and similar to silicon in its bonding motif, which makes it competitive for many applications, none of the allotropes are suitable for certain optoelectronic applications such as photovoltaic (PV) solar cells, for which direct band gaps between 1.0 and 1.5 eV are optimal.[16]

The sp^3 hybridization in diamond gives a large band gap ~5.5 eV while the sp^2 hybridization in graphene has a zero band gap. If one can mix the sp^2-sp^3 carbon allotropes in some form, the result may possess intermediate band gaps and provide an opportunity for "engineered" electronic and optical properties. Experiments show that by compressing different raw sp^2 carbons allotropes, hybrid sp^2-sp^3 phases can be formed[17-22]. Ab initio calculations predicted two metallic phases with sp^2 and sp^3 hybridization, T6 and T14 carbon[23]. Hybrid sp^2-sp^3 carbon allotropes were also proposed as possible structures of cold compressed graphite, unfortunately the resulting band gaps are still either too large or too small for the PV application[24]. However, those studies indicated that hybrid sp^2-sp^3 carbon allotropes may display drastically different electronic and optical properties.

If sp^2-sp^3 mixed hybridization in carbon materials can be engineered with tunable the band gaps in the range 1.0-1.5 eV, it becomes possible to design new carbon allotropes that may be ideal solar cell absorber materials, in contrast to all currently known carbon allotropes.

For decades, silicon based solar cell panels have dominated the PV market, but silicon is an indirect-gap material and a weak absorber of visible light, even though great amounts of efforts have been made to find direct band gap silicon.[25-29] Later, continuous efforts were made to find direct-band-gap absorber materials such as $CuIn_xGa_{1-x}Se_2$, CdTe and inorganic-organic hybrid perovskite compounds ($CH_3NH_3PbX_3$, X=I, Br and Cl).[3-32] All of these PV materials suffer from significant drawback, e.g., In is a rare element,[33-35] Cd and Pb are toxic, and $CH_3NH_3PbX_3$ is not stable. Compared to these absorber materials, hybrid sp^2-sp^3 carbon allotropes could be better candidates because they are abundant, non-toxic, cheap, and most importantly, offering tunable band gaps.

Here, we propose new hybrid sp^2-sp^3 carbon allotropes for PV application using a state-of-art inverse band structure design approach. By incorporating the carbon sp^2 atoms into a sp^3 carbon matrix, we can create a band gap and also tune it by adjusting the size and distribution of the sp^2 atoms, taking advantage of the quantum confinement effect. Combining the multi-objective (MO) optimization with density functional theory calculation implemented in IM^{2}ODE (Inverse Design of Materials by MO Differential Evolution) package, [36, 37] we obtain five new carbon allotropes with direct or quasi-direct band gap ranging from 1.01 to 1.58 eV, which are appropriate for the photovoltaic application. Among these carbon allotropes, C_{10}-C may be a strong candidate as the light absorber material in thin-film solar cells with efficiency as high as that of the expensive crystalline GaAs solar cells.

II. Computational Methods

A. Crystal structures predicted by multi-objective differential evolution

We applied a multi-dimensional global optimization algorithm, as implemented in the IM^{2}ODE package that we developed recently, to design carbon allotropes with direct band gap suitable for solar absorption. Following the general procedure of multi-objective differential evolution (MODE), the package is able to find a set of solutions with both desired properties and relatively low energies. Local optimization of the atomic coordinates and lattice parameters are performed. From the calculated

electronic band structure, we are able to determine the fundamental gap (E_g^g) and direct gap (E_g^d). A material is identified to be a direct gap system when $E_g^g = E_g^d$. In order to find materials with a targeted direct band gap E_g^{opt}, the fitness functions are defined as,

$$\min z_1 = total\ energy \quad (1)$$

$$\min z_2 = \left|E_g^{opt} - E_g^d\right| + \left|E_g^d - E_g^g\right| \quad (2)$$

In equation (1), we search for meta-stable structures by minimization of the total energy. In equation (2), the first item aims at finding materials with direct band gap close to E_g^{opt}, and the second item aims at finding direct band gap materials. The transition matrix element between the valence band maximum (VBM) and conduction band minimum (CBM) states is also included in the designing process. If the transition at the direct band gap is forbidden, z_2 is set to be infinite to rule out the structures that are optically non-active. Subsequently, the MODE algorithm is performed to select and generate new structures. The number of atoms of the unit cell is enumerated from 2 to 24. In the structure searching progress, the population size is 30 and the number of generations is fixed at 20. The size/shape of the unit cell is updated with the lowest energy each generation. The objective direct band gap E_g^{opt} is set to 0.7 eV in the LDA calculation due to its underestimating of the band gap. For the structures that satisfy $z_1 \leq -9.3\ eV/atom$ (which is 0.8 eV/atom higher than that of diamond) and $z_2 \leq 1.0$ eV, the optical properties and the value of band gaps are re-calculated by using the HSE hybrid functional which was found to give accurate band gaps for many semiconductors[38, 39]. The distribution of the structures is shown in Figure S1.

B. Density functional theory calculations

Density functional theory (DFT) method is applied for structural relaxation and the electronic structure calculation. The ion-electron interaction is treated by the projector augmented-wave (PAW) technique[40], as implemented in the Vienna *Ab initio* Simulation Package (VASP)[41]. Moreover, the local-density approximation (LDA)[42] is

adopted to calculate total energies and relax structures. The plane wave cutoff of 500 eV was used, and the Monkhorst-Pack grid with a maximum spacing of $2\pi \times 0.04\text{Å}^{-1}$ was employed in the calculations. In the IM^{2}ODE searching process, we also use LDA to estimate the band gaps of the specific structure to make the calculations affordable although LDA is well-known to underestimate the band gap. Then, the band gap and properties are re-computed by employing the HSE06 functional, which was found to give more accurate band gaps than LDA for semiconductors.[43] The optical matrix elements are calculated using the method of Adolph *et al*.[44, 45] The calculation of the maximum efficiency is based on the improved Shockley-Queisser method[46, 47]. The standard AM1.5G solar spectrum at 25^{o}C is applied in the simulation. Detailed steps of the optical properties calculation is provided in the supporting information. Utilizing the frozen phonon method as implemented in phonopy program[48, 49], the phonon calculations are performed to check the dynamic stability of a specific structure.

C. G0W0-BSE calculations

DFT calculations generally give good results for ground state properties, but not for excited states. In this study, quasiparticle (QP) energy calculations with a single shot G0W0 approximation [50] and neutral excitation spectra by solving the Bethe-Salpeter equation (BSE) [51] are both carried out with VASP. The calculation of the dielectric functions proceeds in a number of steps. First, the self-consistent DFT eigenvalues and Kohn-Sham orbitals are obtained based on calculations of PBE functional. Subsequently, the DFT Green's function G0 and dynamically screened interaction W0 are constructed based on DFT eigenvalues. The QP energies are then calculated using first-order perturbation theory. The electron-hole interactions are included in the BSE, at the level of electron-hole exchange and electrostatic interactions. The coupling term is ignored to simplify the calculation, which is referred to as the Tamm-Dancoff approximation (TDA). Calculations are carried out using the primitive cell. The energy cutoff for response function is 266.67 eV. A Γ centered mesh is used for the Brillouin zone integration. For C_{10}-C, C_{14}-C, C_{20}-D, C_{24}-D and C_{24}-C, we use 8×8×8,

8×8×8, 6×6×6, 6×4×6 and 6×4×4 k-point mesh, respectively. The number of band used in the G0W0 calculation is 240 for C_{10}-C and C_{14}-C, and 960 for C_{20}-D, C_{24}-D and C_{24}-C. 16 valance band states and 16 conduction band states are included in the basis for diagonalization of the BSE Hamiltonian of C_{10}-C, which is found to be sufficient to achieve a converged spectrum.

III. Results and discussion

A. Prediction of the hybrid sp^2-sp^3 carbon allotropes

As illustrated in Figure 1, in order to get a carbon allotrope with desired properties, we propose to embed the sp^2 atoms into the sp^3 carbon matrix. The quantum confinement effect opens a finite gap between the π and π* states of the sp^2 atoms. The key problem is to identify the appropriate hybrid sp^2-sp^3 carbon allotrope with a desired direct band gap between 1.0 to 1.5 eV. To this end, we use a general MO global optimization algorithm implemented in our newly developed IM^{2}ODE package.

We find five carbon allotropes which satisfy the following criteria: (1) The band gaps calculated by HSE06 are in the range 1.0~2.0 eV; (2) The structure is dynamically stable without imaginary phonon mode. The crystal structures are shown in Figure 2, and the band gaps and space groups of these structures are listed in Table 1. All the five structures are hybrid sp^2-sp^3 three dimensional bulk materials, and the sp^2 hybridized carbon atoms appears in pair in those structures. The densities of the carbon allotropes are between the density of graphite and diamond. C_{10}-C, C_{14}-C and C_{24}-C, composed of five membered rings and six membered rings with distorted bond angles, and have low symmetry. C_{20}-D and C_{24}-D, whose space groups are No. 127 (*P4/mbm*) and No. 65 (*Cmmm*) respectively, have tunnel-like voids. C_{24}-D is the most porous structure among them. The total energy of the five carbon allotropes are about 0.5~0.6 eV/atom, less stable than diamond, which is close to that (0.51 eV/atom) of metallic carbon T6[23]. The bulk modulus of the five carbon allotropes are calculated by fitting the Birch-Murnaghan equation of states. Both C_{10}-C and C_{20}-D show large bulk

modulli above 300 GPa, indicating high stability. The details are shown in Table S1.

The present hybridized structures are essentially different from those previously reported. [23, 52] Here, as designed, the sp^2 atoms are totally confined by the sp^3 matrix. By breaking the sp^2 network, the p_z electrons of the sp^2 atoms open a gap due to the quantum confinement effect. While in metallic carbon phases the sp^2 atoms form a chain, the metallicity originates from the delocalization of p_z electrons of the sp^2 network.[52] For compressed nanotubes, the change of the bonding feature from sp^2 to sp^3 occurs under pressure.[52] The local sp^3 bonds form in the sp^2 matrix, which is opposite to the present case, where sp^2 bonds are confined in the sp^3 matrix.

B. Electronic structures

The electronic band structures calculated by HSE06 of all five allotropes show direct band gaps or quasi band gaps between 1.0 and 1.6 eV, as shown in Figure 3 and Figure S2, which fall into the optimum value range as suggested by the Shockley-Queisser model[53]. (The primitive Brillouin zones are shown in Figure S3.) C_{14}-C, C_{20}-D and C_{24}-D show direct band gaps, whereas the conduction band minimum (CBM) and valence band maximum (VBM) are located at R, Γ, and Z respectively. The band gaps for those three structures are 1.27, 1.26 and 1.58 eV, respectively. C_{10}-C and C_{24}-C show quasi-direct band gaps. For C_{10}-C, the CBM is near (0.05, 0.05, 0.05) point along the R-Γ direction and VBM is near (0.15, 0, 0) point along the Γ-X direction. For C_{24}-C, the CBM is near (0.35, 0.35, 0.5) and the VBM is near (0.4, 0.4, 0.5) along the Z-R path. The direct band gap for C_{10}-C and C_{24}-C are 1.25 eV and 1.14 eV, and the indirect gaps are 1.01 eV and 1.09 eV, respectively. Starting from the PBE wave functions and eigenvalues, G0W0 calculations[50] are also performed and the calculated fundamental band gaps are close to those from the HSE06 calculations (as listed in Table S2).

The absorption of visible light occurs between the π and π* states in the hybrid sp^2-sp^3 carbon allotropes due to the opening of band gap by quantum confinement. Figure 3c shows the band decomposed charge densities of the VBM and CBM of the C_{10}-C, and similar results for the other four carbon allotropes are in the supporting information (Figure S4). For all the carbon allotropes obtained, both VBM and CBM

states originate from the distorted sp^2 hybridization, i.e., the VBMs are made up of π states while the CBM are made of π^* states, which is similar to that of graphene. However, unlike the graphene, here the sp^2 hybridized carbon atoms only form pairs, and the conjugated π bonds cannot be formed. Given the components of VBM and CBM states, the optical absorption of visible light should result from the π-π* transition. Note that the optical dipole transition between the π and π* states is allowed, similar to the case of graphene, [54, 55] thus such a hybrid sp^2-sp^3 carbon allotrope can be used as light-absorber materials in solar cells. By calculating the transition matrix elements between the VBM and CBM states (table S3), we further confirmed that the optical transition is allowed.

C. Optical absorption

The hybrid sp^2-sp^3 carbon allotropes have larger light absorption coefficients and higher efficiencies in comparison with known light absorbers. The dielectric tensor $\varepsilon_2(\omega)$ can be used to estimate the optical properties of the obtained five carbon allotropes (see Figure S5). We find that the optical absorption in C_{10}-C and C_{24}-C starts at the direct gap transition energy, while C_{14}-C, C_{20}-D and C_{24}-D do not. The difference is caused by the difference in the transition matrix elements of the crystals, and the calculation results in Table S3 shows the values of C_{14}-C, C_{20}-D and C_{24}-D is almost one magnitude smaller than that of C_{10}-C and C_{24}-C. The calculated optical spectra coefficients of the new carbon allotropes are shown in Figure 4a. The optical absorption of GaAs, which has the highest conversion efficiency among all the known single-junction solar cell absorbers, is also shown for comparison. The optical absorption coefficients of C_{10}-C and C_{24}-C are up to one order of magnitude higher than that of GaAs in the visible light range, C_{14}-C and C_{20}-D are similar to that of GaAs, and only C_{24}-D is slightly smaller than GaAs. Since the quantum efficiency of a solar cell is strongly dependent on the optical absorption coefficient, we calculated the maximum efficiencies of the solar absorbers as a function of thickness according to the optical absorption coefficient by the "spectroscopic limited maximum efficiency (SLME)" method[44,46]. The maximum efficiencies of the five carbon allotropes and GaAs are shown in Figure 4b. For C_{10}-C and C_{24}-C, the photovoltaic

efficiencies are estimated to be 33.5% and 32.9% when it is 3 μm thick, respectively, while the Shockley-Queisser limit of the solar cell efficiency is 33.7%.[56] Therefore, C_{10}-C and C_{24}-C could be used as thin-film solar cell absorber material and the thickness of the absorber layer could be as thin as 3 μm, which decreases the possibility of non-radiative recombination because the photogenerated carriers do not have far to travel before being collected. In accordance with the absorption coefficients, the photovoltaic efficiencies of C_{14}-C and C_{20}-D are close to that of GaAs, and C_{24}-D is still lower than that of GaAs. Of course, the realization of such carbon allotrope based solar cell will still depend on device properties.

The HSE06 calculation shows that only C_{10}-C and C_{24}-C are good light absorbers with the absorption coefficient increasing rapidly above the optical gap, especially for C_{10}-C (see Fig. S5 and Table. S3). Therefore, the optical properties of C_{10}-C are studied in more detail. The imaginary part of the macroscopic dielectric function of C_{10}-C is calculated by solving the BSE with the electron-hole interaction considered, as shown in Figure 5(a). Compared with the HSE06 results, the BSE absorption spectrum shows strong exciton effects, which enhance the low-energy part of the absorption spectrum. Furthermore, its optical absorption exhibits obvious anisotropy as a result of the triclinic structure of C_{10}-C. The calculated imaginary part of the dielectric function in x, y and z direction are shown in Figure 5b. Obviously the light absorption in y-direction is much stronger than that in x and z, because the transition between the π and π^* states are mostly along the y direction. Therefore the orientation control of the synthesized C_{10}-C films may be important for achieving high photovoltaic efficiency.

It is interesting to understand why the obtained carbon allotropes show great photovoltaic efficiencies. According to the Fermi Golden rule, the transition probability per unit time for photonic energy $\hbar\omega$ is proportional to the transition matrix elements from the valence band (VB) to the conduction band (CB), and also proportional to the joint density of states (JDOS) at energy $\hbar\omega$.[56] We find that, the transition matrix of C_{10}-C is just slightly larger than that of GaAs, and C_{24}-C is slightly smaller yet than GaAs. However, the JDOSs of all the five carbon allotropes

are greater than that of GaAs, as shown in Figure 6. Therefore, the amazingly large optical absorption of the carbon allotropes can be attributed to the large JDOS, which is due to the π-π* states in carbon allotropes.

D. Stability of the structures

The dynamic stability of the five new carbon allotropes has been confirmed by the phonon spectrum (Figure S6), which does not show any imaginary phonon mode in the entire Brillouin zone. Furthermore, energetics stability is not a problem either. Although the five new carbon allotropes have energies 0.5-0.6 eV/atom higher than diamond, they are more stable than other allotropes such as ultra-thin carbon nanotubes[57]. In fact, many carbon allotropes with rather high energy have been synthesized, e.g., the one dimensional *sp-carbyne*, whose energy is ~1 eV/atom higher than that of diamond[58]. Recently, Q-carbon with both sp^2 and sp^3 hybridization had been synthesized using high-power nanosecond laser pulses at ambient temperatures and pressures in air.[59] Therefore, we expect that C_{10}-C, C_{14}-C, C_{24}-C, C_{20}-D and C_{24}-D could be fabricated in the future, probably using monolayer graphene as a template or by cold compressing carbon nanotube bundles.[60]

IV. Conclusion

In summary, we propose here that hybrid sp^2-sp^3 carbon allotropes with tunable band gaps can be obtained by embedding the sp^2 atoms into the sp^3 matrix. With our own global optimization package (IM^2ODE), we have predicted five hybrid sp^2-sp^3 carbon allotropes with desirable band gaps for photovoltaic application. Among them C_{10}-C is a strong candidate as the light absorber material in solar cells whose photovoltaic efficiency can be as high as 33.5% at 3 μm thickness. Our results pave new way for designing thin-film solar cell materials with higher efficiencies, as well as other useful optoelectronic semiconductors.

Acknowledgements

The authors thank Yang Zhou for completing part of the IM^2ODE package for

MO optimization. Work at Fudan was supported by NSFC, the Special Funds for Major State Basic Research, FANEDD, NCET-10-0351, Research Program of Shanghai Municipality and MOE, Fok Ying Tung Education Foundation, and Program for Professor of Special Appointment (Eastern Scholar).

Reference

[1]Y. Zhu, S. Murali, M.D. Stoller, K. Ganesh, W. Cai, P.J. Ferreira, A. Pirkle, R.M. Wallace, K.A. Cychosz, M. Thommes, Science 332, 1537 (2011).

[2]M. J. Allen, V. C. Tung, and R. B. Kaner, Chem. Rev. 110, 132 (2009).

[3]Y. Zhang, Y.-W. Tan, H.L. Stormer, P. Kim, Nature 438, 201 (2005).

[4]S. Zhang, J. Zhou, Q. Wang, X. Chen, Y. Kawazoe, P. Jena, Proc. Nat. Acad. Sci., 2372 (2015).

[5]X.-L. Sheng, Q.-B. Yan, F. Ye, Q.-R. Zheng, G. Su, Phys. Rev. Lett. 106, 155703 (2011).

[6]Q. Zhu, A.R. Oganov, M.A. Salvadó, P. Pertierra, A.O. Lyakhov, Phys. Rev. B 83, 193410 (2011).

[7]Y. Lin, L. Zhang, H.-k. Mao, P. Chow, Y. Xiao, M. Baldini, J. Shu, W.L. Mao, Phys. Rev. Lett. 107, 175504 (2011).

[8]Y. Liu, G. Wang, Q. Huang, L. Guo, X. Chen, Phys. Rev. Lett. 108, 225505 (2012).

[9]Q. Li, Y. Ma, A.R. Oganov, H. Wang, H. Wang, Y. Xu, T. Cui, H.-K. Mao, G. Zou, Phys. Rev. Lett. 102, 175506 (2009).

[10]S. E. Boulfelfel, Q. Zhu, and A. R. Oganov, J. Superhard Mater. 34, 350 (2012)

[11]R. Zhou, and X. C. Zeng, J. Am. Chem. Soc. 134, 7530 (2012).

[12]K. Umemoto, R.M. Wentzcovitch, S. Saito, T. Miyake, Phys. Rev. Lett. 104, 125504 (2010).

[13]J.-T. Wang, C. Chen, and Y. Kawazoe, Phys. Rev. Lett. 106, 075501 (2011).

[14]H. Niu, X.-Q. Chen, S. Wang, D. Li, W.L. Mao, Y. Li, Phys. Rev. Lett. 108, 135501 (2012).

[15]Z. Zhao, B. Xu, X.-F. Zhou, L.-M. Wang, B. Wen, J. He, Z. Liu, H.-T. Wang, Y. Tian, Phys. Rev. Lett. 107, 215502 (2011).

[16]N. S. Lewis, science 315, 798 (2007).

[17]R. Aust, and H. Drickamer, Science 140, 817 (1963).

[18]Y. Wang, J.E. Panzik, B. Kiefer, K.K. Lee, Sci. Rep. 2, 520(2012).

[19]B. Sundqvist, Advances in Physics 48, 1 (1999).

[20]H. Hirai, and K.-I. Kondo, Science 253, 772 (1991).

[21]M. J. Bucknum, and E. A. Castro, Carbon Bonding and Structures (Springer, 2011), pp. 79.

[22]W.L. Mao, H.-k. Mao, P.J. Eng, T.P. Trainor, M. Newville, C.-C. Kao, D.L. Heinz, J. Shu, Y. Meng, R.J. Hemley, Science 302, 425 (2003).

[23]S. Zhang, Q. Wang, X. Chen, P. Jena, Proc. Nat. Acad. Sci. 110, 18809 (2013).

[24]F.J. Ribeiro, P. Tangney, S.G. Louie, M.L. Cohen, Phys. Rev. B 72, 214109 (2005).

[25] H. J. Xiang, B. Huang, E. Kan, S.-H. Wei, and X. G. Gong, Phys. Rev. Lett. 110, 118702 (2013).

[26] C. Rödl,T. Sander, F. Bechstedt, J. Vidal, P. Olsson, S. Laribi, J.-F. Guillemoles. Phys. Rev. B 92, 045207 (2015).

[27]Q. Wang, B. Xu, J. Sun, H. Liu, Z. Zhao, D. Yu, C. Fan, J. He, J. Am. Chem. Soc. 136, 9826 (2014)

[28]D. Y. Kim, S. Stefanoski, O. O. Kurakevych, T. A. Strobel, Nat. Mater. 14, 169 (2015)

[29]B. Huang, H. X. Deng, H. Lee, M. Yoon, B. G. Sumpter, F. Liu, S. C. Smith, S.-H. Wei, Phys. Rev. X 4, 021029 (2014)

[30]A.M. Gabor, J.R. Tuttle, D.S. Albin, M.A. Contreras, R. Noufi, A.M. Hermann, Appl. Phys. Lett. 65, 198 (1994).

[31]Z. A. Peng, and X. Peng, J. Am. Chem. Soc. 123, 183 (2001).

[32]M. Liu, M. B. Johnston, and H. J. Snaith, Nature 501, 395 (2013).

[33] Y. Xu, and Q. Li, Nanoscale, 3, 3238 (2011)

[34] J. Kano, E. Kobayashi, W. Tongamp, and F. Saito, Chem. Lett. 37, 204 (2008)

[35] Y. T. Wang, C. J. Ho, and H, L, Tsai, Material Transactions, 51, 1735 (2010)

[36] Y.-Y. Zhang, W. Gao, S. Chen, H. Xiang, X.-G. Gong, Comput. Mater. Sci. 98, 51 (2015).

[37] H.-Z. Chen, Y.-Y. Zhang, X. Gong, H. Xiang, J. Phys. Chem. C 118, 2333 (2014).

[38] J. Heyd, G. E. Scuseria, and M. Ernzerhof, J. Chem. Phys. 118, 8207 (2003).

[39] J. Heyd, G. E. Scuseria, and M. Ernzerhof, J. Chem. Phys. 124, 219906 (2006).

[40] P. E. Blöchl, Phys. Rev. B 50, 17953 (1994).

[41] G. Kresse, and J. Hafner, Phys. Rev. B 49, 14251 (1994).

[42] D. M. Ceperley, and B. Alder, Phys. Rev. Lett. 45, 566 (1980).

[43] J. Heyd, G. E. Scuseria, M. Ernzerhof, J. Chem. Phys. 118, 8207−8215 (2003)

[44] B. Adolph, J. Furthmüller, and F. Bechstedt, Phys. Rev. B 63 125108 (2001)

[45] M. Gajdoš, K. Hummer, G. Kresse, J. Furthmüller, and F. Bechstedt, Phys. Rev. B 73, 045112 (2006)

[46] L. Yu, and A. Zunger, Phys. Rev. Lett. 108, 068701 (2012).

[47] L. Yu, R.S. Kokenyesi, D.A. Keszler, A. Zunger, Adv. Energy Mater. 3, 43 (2013).

[48] X. Luo, J. Yang, H. Liu, X. Wu, Y. Wang, Y. Ma, S.-H. Wei, X. Gong, H. Xiang, J. Am. Chem. Soc. 133, 16285 (2011).

[49] A. Togo, F. Oba, and I. Tanaka, Phys. Rev. B 78, 134106 (2008).

[50] M. S. Hybertsen and S. G. Louie, Phys. Rev. B 34, 5390 (1986)[51] G. Onida, L.Reining, and A. Rubio, Rev. Mod. Phys. 74, 601 (2002)[52] M. Hu, Z. Zhao, F. Tian, A.R. Oganov, Q. Wang, M. Xiong, C. Fan, B. Wen, J. He, D. Yu, Sci. Rep. 3, 03077 (2013).

[53] W. Shockley, and H. J. Queisser, J. Appl. Phys. 32, 510 (1961).

[54] A. Grüneis, R. Saito, G.G. Samsonidze, T. Kimura, M.A. Pimenta, A. Jorio, A.G.S. Filho, G. Dresselhaus, M.S. Dresselhaus, Phys. Rev. B 67, 165402 (2003).

[55] L. Matthes, P. Gori, O. Pulci, F. Bechstedt, Phys. Rev. B 87, 035438 (2013).

[56] P. Schattschneider and B. Jouffrey, Energy-Filtering Transmission Electron Micrsocopy, L. Reimer (Ed.), Springer-Verlag, Berlin, Ch.3, 151-224 (1995).

[57] E. Menéndez-Proupin, A. L. Montero-Alejo, and J. M. García de la Vega, Phys. Rev. Lett. 109, 105501 (2012).

[58] W. A. Chalifoux, and R. R. Tykwinski, Nat. Chem. 2, 967 (2010).

[59] J. Narayan, and Anagh Bhaumik, J. Appl. Phys. 118, 215303 (2015)

[60] R. Ruoff, Nature 483, S42 (2012).

Table 1 The structural properties, energies (eV/atom), densities (g/cm^{-3}), and band gaps (eV) of different carbon allotropes.

Crystal	Space group	Formation energy	Density	Direct band gap	Indirect band gap
diamond	*Fd*3*m*	0.00	3.52	6.99	5.31
graphite	*P*6$_3$*mc*	0.00	1.11	0.00	--
C_{10}-C	*P*$\bar{1}$	0.51	3.07	1.25	1.01
C_{14}-C	*P*1	0.55	2.95	1.27	--
C_{20}-D	*P*4/*mbm*	0.55	2.97	1.26	--
C_{24}-D	*Cmmm*	0.58	2.55	1.58	--
C_{24}-C	*P*1	0.68	2.72	1.14	1.09

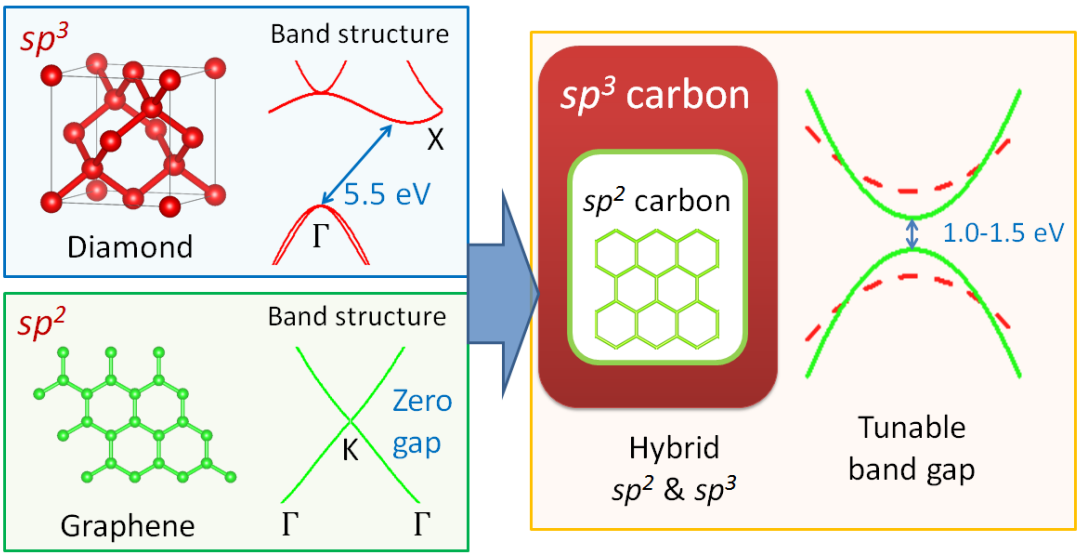

Figure 1 Schematic illustration of the concept of hybrid sp^2-sp^3 carbon allotropes. Hybrid sp^2-sp^3 carbon allotropes may have optimal electronic properties for solar cell absorbers. By embedding the sp^2 atoms into the sp^3 matrix, the band gap of hybrid carbon is tunable through the quantum confinement effect.

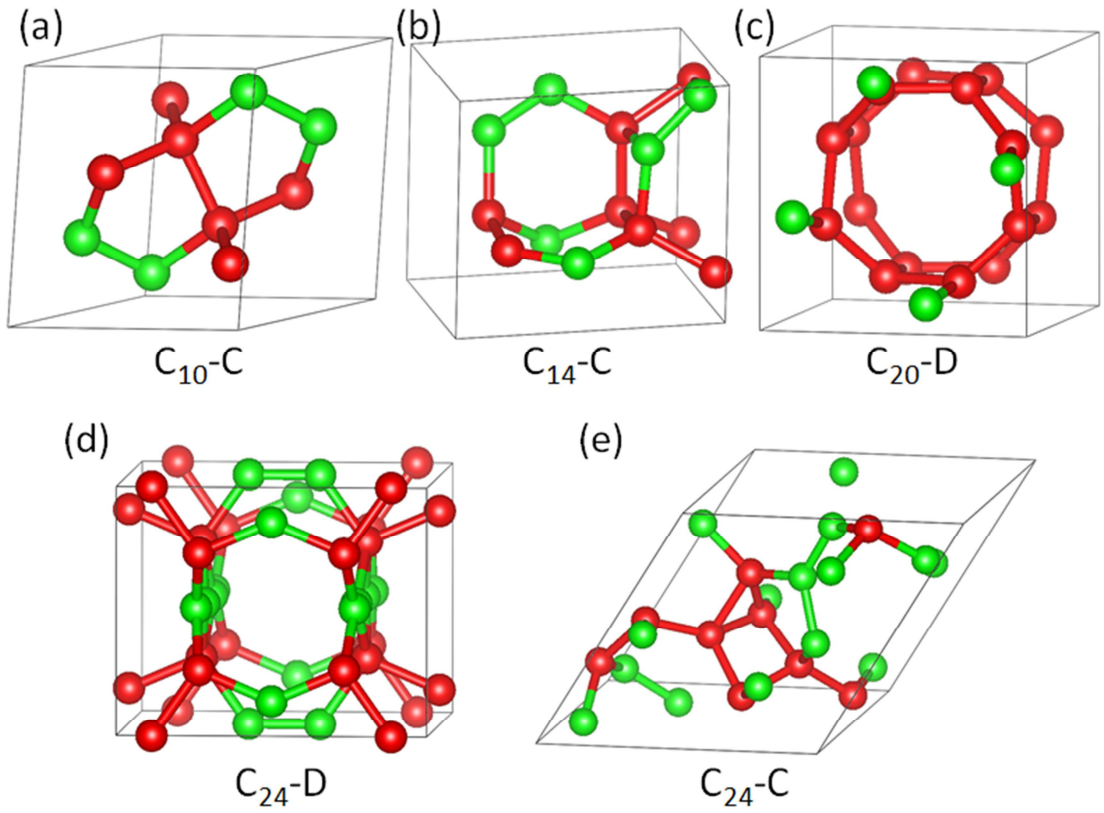

Figure 2. The crystal structures of the five carbon allotropes. (a) C_{10}-C, (b) C_{14}-C, (c) C_{20}-D, (d) C_{24}-D and (e) C_{24}-C. The green and red balls denote three coordinated and four coordinated carbon atoms, respectively. For the naming convention of the carbon allotropes, the number in subscript is the number of atoms in the unit cell and the last character is the crystallographic symbol according to the symmetry of the structure.

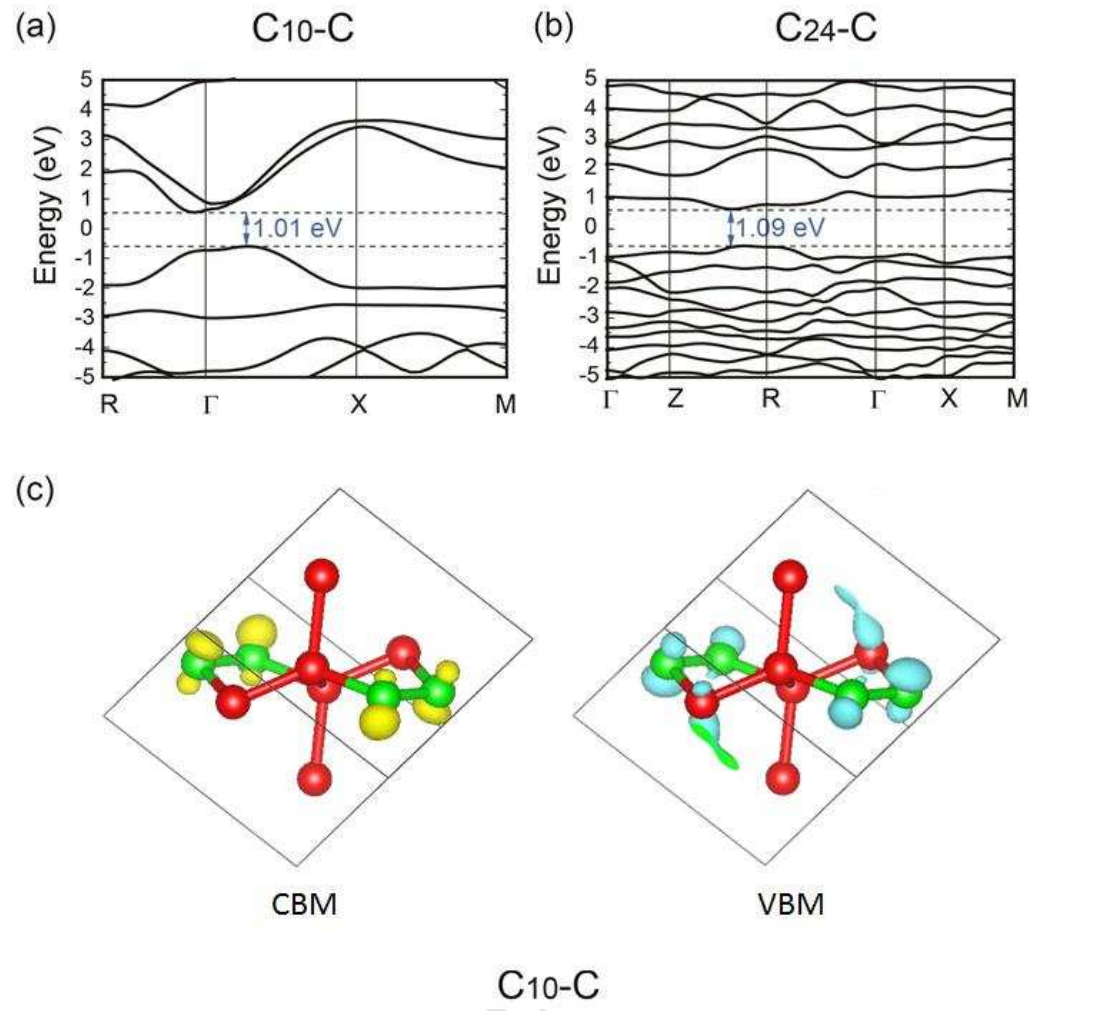

Figure 3. Electronic structures of the carbon allotropes. Band structures of (a) C_{10}-C, (b) C_{24}-C are calculated with the HSE06 functional. The overall VBM and CBM are denoted by a dashed line. (c) The partial charge density of the CBM (yellow) and VBM (blue) states for C_{10}-C. The CBM and VBM states distribute mainly on the sp^2 hybridized carbon atoms (marked as green).

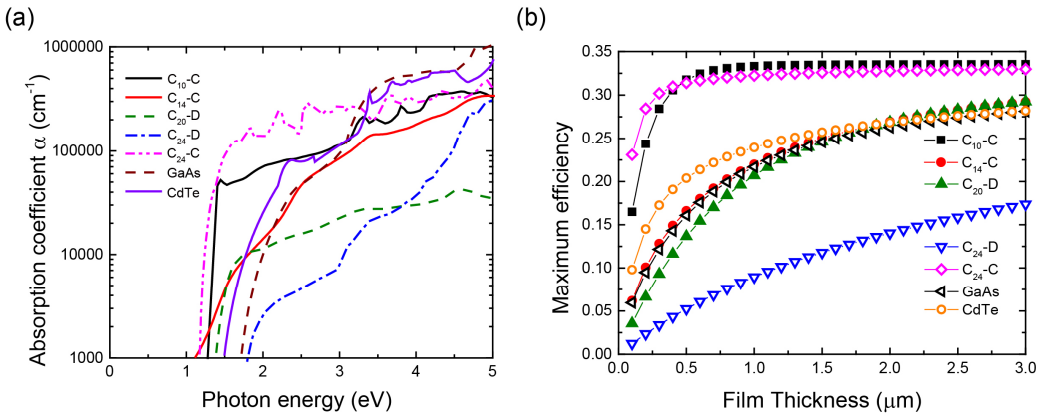

Figure 4. Optical properties of the carbon allotropes. (a) Absorption coefficient and (b) maximum photovoltaic efficiency from the HSE06 calculations. The maximum efficiency of C_{10}-C and C_{24}-C might surpass that of GaAs.

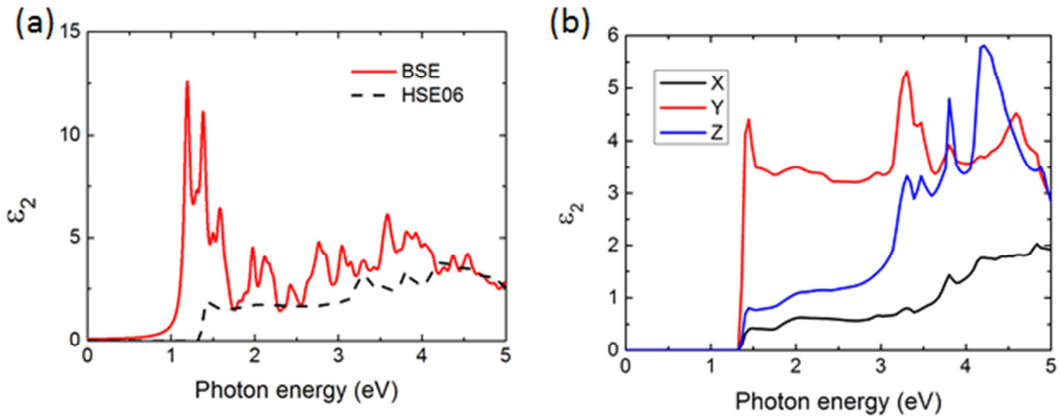

Figure 5. Optical properties of C_{10}-C. (a) Imaginary part of the dielectric function of C_{10}-C from the BSE calculation (red solid line) and HSE06 calculation (black dash line) and (b) Imaginary part of the dielectric function of C_{10}-C from the HSE06 calculation in x, y and z direction. (The x, y and z direction refer to the Cartesian coordinates)

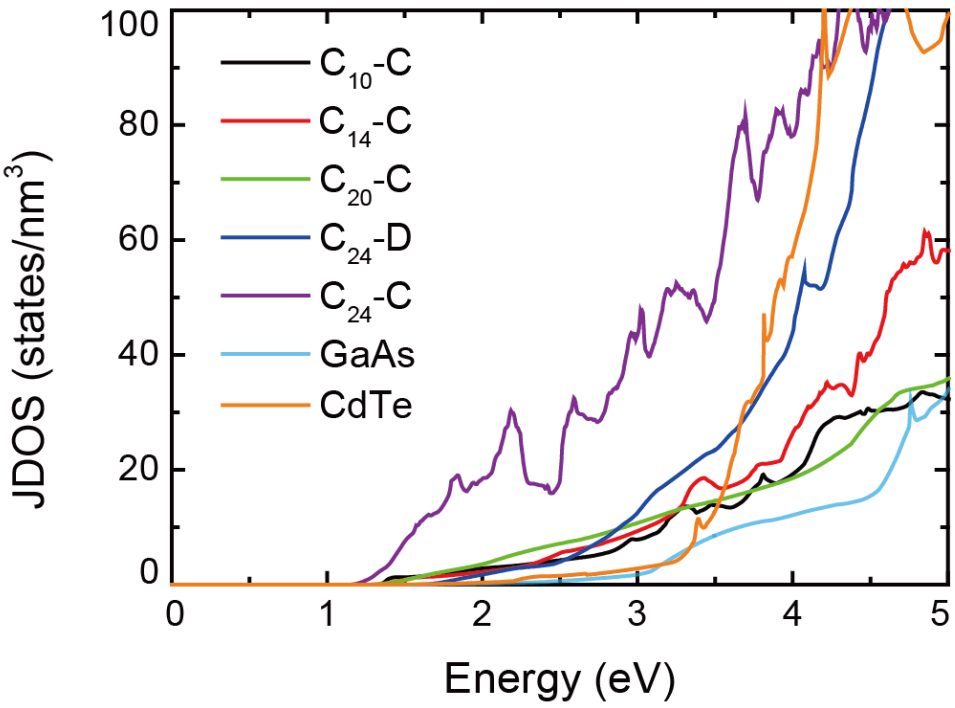

Figure 6. The Joint Density of States (JDOS) of the carbon allotropes. The JDOS for C_{10}-C, C_{14}-C, C_{20}-D, C_{24}-D, and C_{24}-C are calculated by HSE06. GaAs and CdTe are also shown for comparison. The JDOS of all the five carbon allotropes dominates that of GaAs.